frontiers in Materials

ORIGINAL RESEARCH
published: 31 January 2020
doi: 10.3389/fmats.2020.00009

Thermoplastic Starch Composites With Titanium Dioxide and Vancomycin Antibiotic: Preparation, Morphology, Thermomechanical Properties, and Antimicrobial Susceptibility Testing

*Aleksandra Ujcic[1], Sabina Krejcikova[1], Martina Nevoralova[1], Alexander Zhigunov[1], Jiri Dybal[1], Zdenek Krulis[1], Petr Fulin[2], Otakar Nyc[3] and Miroslav Slouf[1]**

[1] Institute of Macromolecular Chemistry, Czech Academy of Sciences, Prague, Czechia, [2] First Orthopedics Clinic of the First Faculty of Medicine of the Charles University, Motol University Hospital, Prague, Czechia, [3] Department of Medical Microbiology, Second Faculty of Medicine of the Charles University, Motol University Hospital, Prague, Czechia

OPEN ACCESS

Edited by:
Andrea Dorigato,
University of Trento, Italy

Reviewed by:
Debora Puglia,
University of Perugia, Italy
Francisco Javier Medel,
University of Zaragoza, Spain
S. M. Sapuan,
Putra Malaysia University, Malaysia

***Correspondence:**
Miroslav Slouf
slouf@imc.cas.cz

Specialty section:
This article was submitted to Polymeric and Composite Materials, a section of the journal Frontiers in Materials

Received: 24 September 2019
Accepted: 09 January 2020
Published: 31 January 2020

Citation:
Ujcic A, Krejcikova S, Nevoralova M, Zhigunov A, Dybal J, Krulis Z, Fulin P, Nyc O and Slouf M (2020) Thermoplastic Starch Composites With Titanium Dioxide and Vancomycin Antibiotic: Preparation, Morphology, Thermomechanical Properties, and Antimicrobial Susceptibility Testing. Front. Mater. 7:9. doi: 10.3389/fmats.2020.00009

Biodegradable composites of thermoplastic starch (TPS), titanium dioxide particles (TiO_2; average size 0.2 μm), and/or antibiotic (ATB; vancomycin) were prepared. Light and electron microscopy demonstrated that our recently developed, two-step preparation procedure yielded highly homogeneous TPS matrix with well-dispersed TiO_2 particles even for high filler concentrations (up to 20%). Oscillatory shear rheometry showed an increase in viscosity of TPS after addition of TiO_2 and ATB (from ca 2×10^5 Pa·s to ca 1×10^6 Pa·s at 1 rad/s and 120°C). However, the high viscosity of TPS/TiO_2/ATB composites did not prevent reproducible preparation of the composites by melt-mixing. Dynamic mechanical analysis proved a significant increase in shear moduli (storage, loss and complex modulus) of TPS after addition of TiO_2 and ATB (storage modulus increased from ca 25 MPa to more than 600 MPa at 1.33 rad/s at room temperature). Both rheological and mechanical properties indicated strong interactions among TPS matrix, filler, and antibiotics. The final TPS composites were soft enough to be cut with a sharp blade at room temperature, the TPS matrix was fully biodegradable, the TiO_2 filler was biocompatible, and the ATB could be released locally during the matrix degradation. Selected samples were tested for bacterial susceptibility using standard tube dilution test and disk diffusion test. The results proved that the ATB retained its bacteriostatic properties after the thermal processing of the composites. Therefore, the prepared TPS/TiO_2/ATB composites represent a promising material for biomedical applications related to the local release of antibiotics.

Keywords: thermoplastic starch, morphology, thermomechanical properties, local release of antibiotics, antibacterial activity

INTRODUCTION

Starch-based materials are attractive due to their biodegradability and wide range of applications, such as packaging, coating, agriculture, medicine, pharmacy, or even optoelectronics (Sarka et al., 2011, 2012; Saiah et al., 2012; Xie et al., 2013; Ghavimi et al., 2015; Oleyaei et al., 2016a; Campos-Requena et al., 2017; Dufresne and Castano, 2017; Javanbakht and Namazi, 2017; Kuswandi, 2017; Liu G. et al., 2017; Liu S. et al., 2017; Sarka and Dvoracek, 2017, Ilyas et al., 2018, Ilyas et al., 2019). However, the melting temperature of native starch is higher than its degradation temperature. Consequently, for most applications, it is necessary to transform the granular starch into an amorphous and homogenous thermoplastic matrix (Biliaderis, 2009; Bertolini, 2010; Visakh et al., 2012; Abral et al., 2019). Starch plasticization has been intensively investigated by many authors (Aichholzer and Fritz, 1998; Huang et al., 2005; Dai et al., 2008; Li et al., 2008; Pushpadass et al., 2008; Xie et al., 2012; Ostafinska et al., 2017). The results of these investigations showed that the preparation of thermoplastic starch (TPS) depended on many factors, such as the starch source (e.g., wheat, corn, and potato; Ao and Jane, 2007; Bertolini, 2010), plasticizer type (Dai et al., 2008; Pushpadass et al., 2008), and processing method (Altskar et al., 2008). The majority of starch-based composites have been prepared by single-step solution casting (SC; Campos et al., 2017; Dufresne and Castano, 2017; Guz et al., 2017; Javanbakht and Namazi, 2017; Liu S. et al., 2017; Pelissari et al., 2017; Ali et al., 2018; Abral et al., 2019) or single-step melt mixing (MM; Campos-Requena et al., 2017; Olivato et al., 2017). The TPS materials prepared by the above-mentioned single-step procedures were found to be homogeneous at the macroscopic level but showed various inhomogeneities, such as non-fully plasticized starch granules, at the microscopic level. Nevertheless, our recent work (Ostafinska et al., 2017) has demonstrated that a two-step procedure based on solution casting and subsequent melt mixing resulted in a highly homogeneous TPS matrix with very homogeneous dispersion of TiO_2 particles.

Significant attention has been devoted in the recent literature to the TPS-based composites with different kinds of fillers (Xie et al., 2013). This work is focused on TPS composites with titanium dioxide, with high content of filler (>10 wt.%), which have not been studied so far according to available literature, as summarized below. Common fillers employed in TPS composites comprise clays (Carvahlo et al., 2001; Dai et al., 2012; Kelnar et al., 2013; Oleyaei et al., 2016a; Campos-Requena et al., 2017; Olivato et al., 2017), graphene (Javanbakht and Namazi, 2017), carbon nanotubes (CNT) (Liu S. et al., 2017), natural fibers (Svagan et al., 2009; Campos et al., 2017; Kargarzadeh et al., 2017; Pelissari et al., 2017; Ilyas et al., 2018, 2019), polysaccharide-based crystals (Dufresne and Castano, 2017; Ali et al., 2018), and metal oxides and chalcogenides (Oleyaei et al., 2016b; Guz et al., 2017; Liu et al., 2018). Titanium dioxide (TiO_2) represents attractive filler in materials for biomedical applications due to its biocompatibility with bone cells and tissues (Webster et al., 1999, 2000; Sengottuvelan et al., 2017). This material has been widely studied in biodegradable composites, such as PLA/TiO_2 (Boccaccini et al., 2005), PLA/TiO_2-Bioglass (Boccaccini and Blaker, 2006), PLA/PCL/TiO_2 (Mofokeng and Luyt, 2015a,b; Ostafinska et al., 2015), and PCL/TiO_2 (Tamjid et al., 2011; Gupta et al., 2012; Vackova et al., 2017). Nevertheless, just little information is currently available regarding the effects of TiO_2 on the properties of thermoplastic starch. Yun et al. (2012) investigated starch/polyvinyl alcohol/TiO_2 (5–15 wt.%) nanocomposites that show photocatalytic activity under UV and visible light irradiation. Fei et al. (2013) studied the influence of TiO_2 (0–8 wt.%) on the structure of TPS/polycaprolactone (PCL) blends. Razali et al. (2016) prepared TPS/TiO_2 (1 wt.%) composites reinforced with Donax grandis hypodermal fiber (DGHF) by solution casting followed by compression molding. These researchers reported that the addition of DGHF to TPS led to structural changes and increased the crystallinity of the composites. Furthermore, the addition of TiO_2 enhanced the crystallinity and resulted in a coarse fiber surface. Oleyaei et al. (2016a,b) studied TPS-based nanocomposites (prepared by solution casting) with the addition of TiO_2 (0.5–2 wt.%), and the same composites with the addition of both TiO_2 and sodium montmorillonite (MMT). They found that maximum improvement in mechanical properties for the TPS/TiO_2 composite was achieved for 1% of the filler, whereas for TPS/TiO_2/MMT the best results were obtained for 2 wt.% of TiO_2 and 3 wt.% of MMT. Furthermore, our recent study (Ostafinska et al., 2017) reported on the addition of low amounts of TiO_2 (0–3 wt.%) to TPS. It was demonstrated that the TiO_2 particles changed the crystallinity and rheological properties slightly due to the partial degradation of the TPS matrix during melt mixing.

In this work, we focused our attention on TPS/TiO_2 composites with higher filler content (up to 20%) that have not been reported in the literature to date. We wanted to verify that the previously described two-step preparation protocol of TPS composites, which yielded highly homogeneous TPS/TiO_2 systems for up to 3% of the filler (Ostafinska et al., 2017) will also be effective for the preparation of highly loaded TPS/TiO_2 composites. Moreover, we investigated whether the combination of a high-viscosity TPS matrix and a high filler concentration will result in a material with good thermomechanical properties that can be prepared using standard solution casting and melt mixing procedures. Finally, we prepared TPS/ATB and TPS/TiO_2/ATB composites in order to verify that thermally resistant antibiotics, such as vancomycin, can survive our two-step plasticization process and filler addition without losing their antibacterial activity.

EXPERIMENTAL

Materials

Wheat A-starch (S) was supplied by Amylon a.s., Czech Republic (type Soltex NP1; amylose content ∼25%; particle size 5–25 μm; total solids: 88.5%—CSN EN ISO 1666; SEM micrograph of the source starch shown in **Figure S1**). Anhydrous glycerol (G; min. 99%), hydrochloric acid (HCl; 35%) and sodium bromide (reagent grade; min. 99%) were obtained from Lach-Ner, Czech Republic. Commercial titanium dioxide (TiO_2; anatase, particles size 50–200 nm) was provided by Sigma-Aldrich, USA. The commercially available vancomycin antibiotic

TABLE 1 | List of the prepared TPS-based composites.

Sample	S (wt.%)	G (wt.%)	TiX (wt.%)	ATB (wt.%)
TPS	70	30	–	–
TPS/TiO_2 (10%)	63.2	26.8	10	–
TPS/TiO_2 (20%)	56.2	23.8	20	–
TPS/ATB	63.2	26.8	–	10
TPS/TiO_2/ATB	56.2	23.8	10	10

All samples contain residual water after processing by solution casting and melt mixing (∼5%).

(ATB; Vancomycin Mylan, obtained from Biologici Italia, Italy) was used in ATB-loaded composites.

Preparation of TPS/TiO_2/ATB Composites

All of the samples (**Table 1**) were prepared by the two-step method consisting of solution casting (SC) followed by melt mixing (MM) as described in more detail in our previous report (Ostafinska et al., 2017). All of the chemicals used for the sample preparation (see previous section) were stored in a refrigerator in order to minimize their possible degradation (which might be a problem especially for the biodegradable starch powder). Briefly, the samples were made by SC using a starch/glycerol ratio of 70/30 (wt.%) and starch/water ratio of 1/6. At first, starch powder, TiO_2 and/or ATB were dispersed in water using an ultrasonic bath for 1 min, and then the glycerol was added for 2 min. The prepared water suspension (starch with glycerol and all additives, which was premixed for 30 min at room temperature) was mixed at an elevated temperature until the viscosity increased significantly (at least 10 min at a temperature above 65°C), and the mixture became visually homogeneous. Then the solution was cast onto thin foils and dried at the ambient temperature for 2–3 days followed by storage for 4 days in a desiccator with a supersaturated NaBr solution (relative humidity = RH = 57%). The dried SC samples were melt mixed (5 min, 110°C, 100 rpm) in a microextruder (μ-processing DSM, Netherlands) and compression molded (SC + MM samples) at 110°C (4 min at 50 kN + 2 min at 150 kN) in a special frame by a hydraulic press (Fontijne Grotnes, Netherlands). Since the properties of the TPS samples are very sensitive to humidity, all of the samples were stored in a desiccator with a supersaturated NaBr solution immediately after the preparation and between all experiments. The aging of samples was performed at the same conditions, i.e., the samples were kept 6 months at ambient temperature, closed in a desiccator with supersaturated NaBr solution.

Characterization of TPS/TiO_2/ATB Composites

Light Microscopy

The overall homogeneity of the filler dispersion at lower magnifications was checked using a light microscope (Nikon Eclipse 80i; Nikon, Japan). Thin sections (∼40 μm) were cut with a rotary microtome (RM 2155; Leica, Germany), placed in oil between the support and cover glasses and observed with transmitted light using bright field imaging.

Scanning Electron Microscopy

Morphology of the TPS matrix and composites at higher magnifications was visualized with a high resolution field-emission gun scanning electron microscope (SEM) (Quanta 200 FEG; FEI, Czech Republic) using secondary electron imaging (SEM/SE) and backscattered electron imaging (SEM/BSE) at 5–30 kV. The samples were broken in liquid nitrogen (below the glass transition temperature of TPS), fixed on a metallic support using silver paste (Leitsilber G302, Christine Groepl, Austria), and the fracture surfaces were covered with a thin Pt layer (∼8 nm; vacuum sputter coater, SCD 050, Balzers, Liechtenstein). The SEM/SE and SEM/BSE micrographs showed mostly topographic and material contrast, respectively.

Attenuated Total Reflectance Infrared Spectroscopy

Infrared spectra of TiO_2, TPS, and composites (after preparation and after 6 months) were acquired with a Golden Gate single reflection attenuated total reflectance cell (ATR; Specac, Ltd., Orpington, Kent, UK) using a Fourier transform infrared spectrometer (FTIR; Thermo Nicolet Nexus 870; Thermo Fisher Scientific Inc., Waltham, Massachusetts, USA) purged with dry air. The spectrometer was equipped with a liquid nitrogen cooled mercury cadmium telluride (MCT) detector, and the ATR cell employed a diamond internal reflection element. The ATR FTIR spectra were recorded with a resolution of 4 cm^{-1}, and 256 scans were averaged per spectrum. After subtraction of the spectrum of the atmosphere, the baselines were corrected (linear baseline correction) and an advanced ATR correction was applied (the correction is defined and recommended within the control FTIR software OMNIC).

Wide-Angle X-Ray Scattering (WAXS)

Diffraction patterns were obtained using an Explorer high-resolution diffractometer (GNR Analytical Instruments, Italy). This instrument was equipped with a one-dimensional silicon strip detector Mythen 1K (Dectris, Switzerland). Samples were measured in a reflection mode. CuKα radiation (wavelength λ = 1.54 Å) monochromatized with a Ni foil (β filter) was used for diffraction experiments. The measurements were performed in the 2θ range of 3 to 50° with a step of 0.1°. The exposure time at each step was 10 s. The peak deconvolution procedure was carried out using the Fityk software (Wojdyr, 2010). The peak positions were employed to obtain the periodicities according to Bragg's law, $d = \lambda/2\sin\theta$, where λ was the X-ray wavelength and θ was the scattering angle. Crystallinities were estimated using the integral intensities of the diffraction signals of the crystalline (I_c) and amorphous (I_a) phases $CR = I_c/(I_c + I_a)$.

Rheometry

Rheological properties were studied in oscillatory shear flow using a Physica MCR 501 rheometer (Anton Paar GmbH, Austria). Special anti-slipping parallel-plate geometry of 25 mm diameter plates was used. The sample thickness was ∼1 mm. The experiments were performed at 120°C

in the linear viscoelastic range (LVE range), confirmed by a strain sweep test at the frequency of 1 Hz. Dynamic frequency sweeps tests were carried out for the frequency range of 10^{-1}–10^{2} rad/s at a strain of 0.05%. Each sample was measured at least three times and the results were averaged.

Dynamic Mechanical Analysis

Mechanical properties were evaluated by dynamic-mechanical analysis (DMA). The linear viscoelastic characteristics—the absolute value of complex modulus $|G^*|$, storage G', loss modulus G'' and loss factor tan(δ)—were measured in the rectangular torsion mode using a Physica MCR 501 rheometer (Anton Paar GmbH, Austria). First, the strain amplitude sweep tests were conducted at the frequency 1 Hz in order to determine the linear viscoelastic range of the TPS matrix and all of the TPS/TiO_2/ATB composites. Then, two types of experiments were performed: frequency sweeps and temperature sweeps. The frequency sweep measurements were carried out at room temperature (23°C) in the frequency range of 10^{-1} to 10^{2} rad/s, the strain was set to 0.1%, and the results of at least two specimens with the dimensions of 20 × 10 × 1.5 mm were averaged. The temperature sweep measurements were carried out in the temperature range of −90 to 100°C (with a heating rate of 5°C/min), at a strain of 0.05%, and angular frequency of 6.28 rad/s. Each sample was measured at least three times and the results were averaged.

Antimicrobial Susceptibility Testing of TPS/TiO_2/ATB Composites

The classical microbiological tube dilution test and disk diffusion test were used to evaluate the antimicrobial susceptibility (activity) as described elsewhere (Jorgensen and Ferraro, 2009). Both TPS/ATB and TPS/TiO_2/ATB composites were used for these experiments. In the tube dilution test, the samples were dispersed into tubes containing 5 ml of Mueller Hinton broth (Oxoid; Czech Republic). The resulting concentration of vancomycin in the polymer was 32 mg/L. The injectable vancomycin was diluted in the same medium to achieve the concentration of 32 mg/L as well. All of the tested tubes including the control sample without the antibiotics were inoculated with a standardized bacterial suspension of the CCM 4223 *Staphylococcus aureus* reference strain (density according to McFarland = 1). In disk diffusion method, the samples were slightly pushed into Mueller Hinton (Oxoid; Czech Republic) agar surface inoculated with suspension of the reference strain CCM 4223 *Staphylococcus aureus* in saline (density according to McFarland = 0.5) and the inhibitory zone was observed. Each test was performed two times in order to verify the reproducibility.

RESULTS AND DISCUSSION

Morphology of TPS Composites

TPS/TiO_2 and TPS/TiO_2/ATB composites after solution casting (SC) and melt mixing (SC + MM) (**Table 1**) were observed by

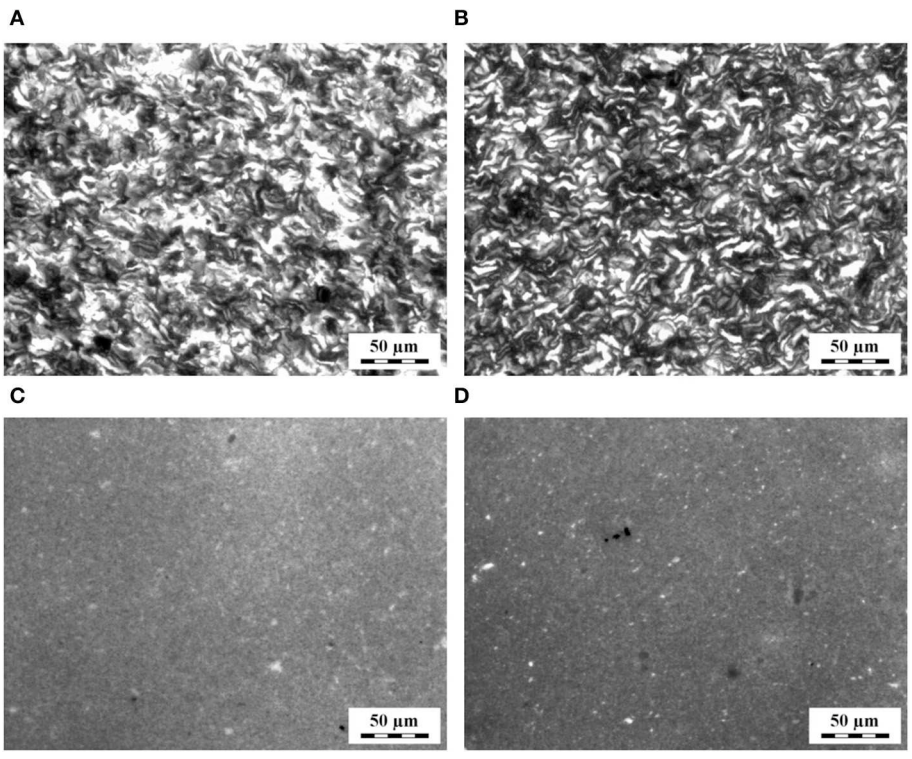

FIGURE 1 | LM micrographs showing the structure of the TPS/TiO_2 composites with **(A,C)** 10% and **(B,D)** 20% of the filler: **(A,B)** after solution casting and **(C,D)** after solution casting and melt mixing.

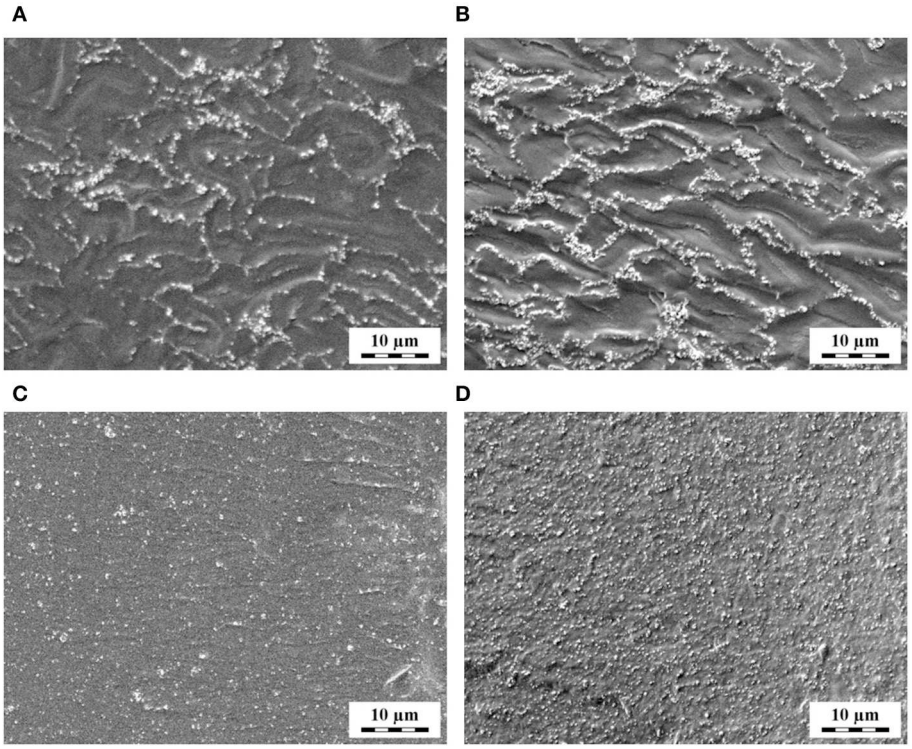

FIGURE 2 | SEM/SE micrographs showing TPS/TiO_2 composites with **(A,C)** 10% and **(B,D)** 20% of the filler: **(A,B)** after solution casting and **(C,D)** after solution casting and melt mixing.

LM (**Figure 1**) and SEM (**Figure 2**). The lower magnification LM micrographs proved that the large agglomerates of TiO_2 particles, which were formed after SC (**Figures 1A,B**) were destroyed after SC + MM (**Figures 1C,D**). The higher magnification SEM micrographs showed that the TiO_2 particles tended to envelop the plasticized but not-fully merged starch granules after SC (**Figures 2A,B**), while the subsequent MM step resulted in the complete merging of starch granules and a highly homogeneous distribution of the TiO_2 nanoparticles (**Figures 2C,D**).

Both LM and SEM micrographs confirmed that the two-step preparation (SC + MM) was necessary to obtain fully plasticized starch with a homogeneously dispersed filler (up to 20 wt.%). SC led to non-fully merged starch granules, while MM alone resulted in non-plasticized granules and/or their agglomerates in the TPS matrix (**Figure S2**). This finding was in agreement with the results of our previous work (Ostafinska et al., 2017) on the TPS/TiO_2 composites with lower filler amounts (up to 3%). The morphological study also proved that the addition of ATB (up to 10 wt.%) had no effect on the morphology of the TPS matrix and on the dispersion of TiO_2 particles (**Figure S3**). Further morphological results suggested that even higher concentrations of TiO_2 (up to 25%) could be dispersed in the TPS matrix using our two-step SC + MM method (**Figure S4**) but the particles began to agglomerate and the viscosity of the composites increased too much, preventing their reproducible preparation and reliable rheological characterization.

IR and WAXS Characterization of TPS Composites

The changes in the structure between the native starch and the thermoplastic starch (after SC and after SC+MM) were studied in detail in our previous work (Ostafinska et al., 2017). In the present work, we characterized the structure of the TPS/TiO_2 composites prepared by SC+MM and their changes during aging. **Figure 3** shows ATR FTIR spectra of the composites together with the spectrum of the starch powder. The figure displays the bands in the 1,100–900 cm^{-1} region (C–O, C–C stretching, and C–O–H bending), which were shown to be sensitive to the changes in the crystalline structure of the starch (Capron et al., 2007): the intensity of the band at 1,022 cm^{-1} appeared to increase in more amorphous samples, while the bands at 1,000 and 1,047 cm^{-1} became more defined in more crystalline samples. In a recent study (Warren et al., 2016), it was shown that the relationship between the infrared spectra of the starches with different degrees of order is more complex than it had been previously appreciated; nevertheless, it was also confirmed that the main difference between the starches with high and low degrees of order is a shift of the band at 1,020 cm^{-1} to higher wavenumbers (Warren et al., 2016). As presented in **Figure 3**, our results showed that compared to the starch powder with the band at 1,020 cm^{-1}, the FTIR spectra of the composites exhibited a shift of that band to 1,027 cm^{-1}, while the relative intensities of the bands at 1,047 and 998 cm^{-1} decreased. This is explained

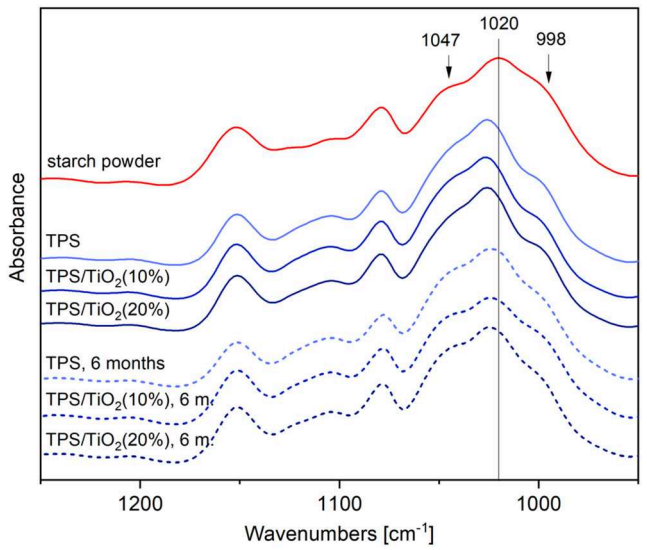

FIGURE 3 | IR spectra of TPS and TPS/TiO_2 composites after preparation and after 6 months of aging; the peaks at 998, 1020, and 1047 cm^{-1} are connected with the changes of crystalline structure of the TPS matrix.

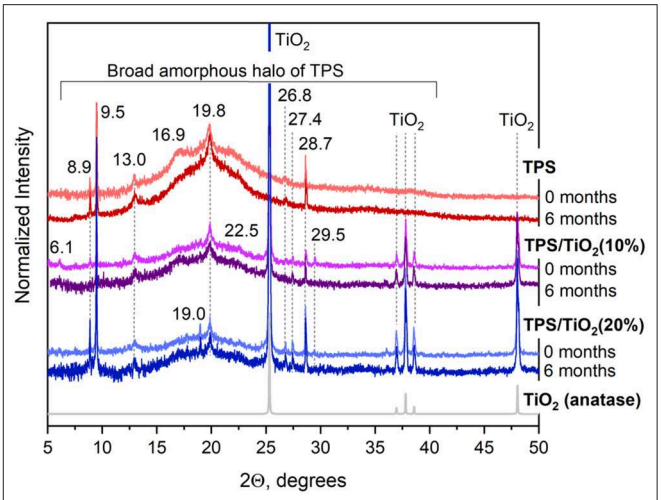

FIGURE 4 | X-ray diffraction patterns of TPS and TPS/TiO_2 composites after preparation and after 6 months of aging. The diffraction pattern at the bottom is theoretically calculated diffractogram of anatase modification of titanium dioxide. The peaks of TPS are marked with their 2θ values.

by the decrease in the crystallinity (short range ordering) of the starch in the composites, in agreement with our previous report (Ostafinska et al., 2017). Upon aging of the composites, small changes of the TPS crystalline structure could be observed: The central band in the FTIR spectra was shifted back in the direction of lower wavenumbers to 1,025 cm^{-1} and the intensities of the bands at 1,047 and 998 cm^{-1} increased, indicating an increase in ordering and recrystallization. Furthermore, the IR/ATR data suggested that the addition of TiO_2 and ATB did not influence the TPS matrix structure (**Figure S5**).

WAXS patterns are summarized in **Figure 4**. The diffractograms were normalized approximately to the same noise and then to the intensity of characteristic triplet of diffraction of TiO_2 anatase form (the three diffractions around $2\theta = 38°$). The diffraction peak positions of neat TPS were in reasonable agreement with the results of previous studies (Soest et al., 1996; Ostafinska et al., 2017). All TPS/TiO_2 composites showed sharp peaks corresponding TiO_2. The TPS crystalline structure did not change with time significantly as evidenced by the fact that most of the TPS diffraction peaks retained their positions and intensities. The moderate changes of crystalline structure were in agreement with FTIR results (**Figure 3**). One notable change was associated with the neat TPS sample, where the peak at $2\theta = 16.9°$ became much more pronounced after 6 months of aging. This corresponded to the starch crystallization into V_H type crystals (retrogradation; Zobel et al., 1967; Rappenecker and Zugenmaier, 1981; Soest et al., 1996; Ilyas et al., 2018). Interestingly, this change was not observed in the TPS/TiO_2 composites, suggesting that the higher concentration of TiO_2 particles prevented standard TPS retrogradation and resulted in the formation of different crystalline structures that were not stable with time, as discussed below. A few lower-intensity TPS diffractions (mostly at $2\theta > 25°$) were observed for TPS/TiO_2 composites in comparison with neat TPS, which confirmed that TiO_2 nanoparticles somewhat influenced the crystalline structure of TPS matrix. The overall TPS crystallinity *increased* with the addition of TiO_2 and then it *slightly decreased* after 6 months of aging. After the preparation, the neat TPS exhibited the crystallinity of 6.5%, whereas TPS/TiO_2 (10%) and TPS/TiO_2 (20%) showed the crystallinity of 9.8 and 24.8%, respectively. After 6 months of aging, the crystallinity of the neat TPS increased slightly (although the change from 6.5 to 6.8% was within experimental and/or fitting procedure error), while the crystallinities of the TPS/TiO_2 (10%) and TPS/TiO_2 (20%) composites somewhat decreased to 7.7 and 18.9%, respectively. Our tentative explanation consists in that TiO_2 particles promoted the ordering and crystallization of the starch during the *plasticization process*, but the TiO_2-induced crystalline structures were metastable and during the *aging process* were slowly destroyed by the plasticizer molecules. The concentration of plasticizer in TPS was almost constant as demonstrated by an independent TGA analysis (**Figure S6**). This explanation is supported by the fact that the observed changes (i.e., both TiO_2-induced increase in crystallization and the subsequent decrease in the crystallization during aging) were more intense for higher TiO_2 particle concentrations. In TPS composites with lower filler concentrations (and in the neat TPS observed in this work), the crystallinity tends to increase with time (Mina et al., 2012; Wang et al., 2015). However, in the TPS/TiO_2 composites with higher filler concentrations the crystallinity showed a reversed trend, as unambiguously proved by WAXS.

For neat TPS, both ATR FTIR and WAXS methods were in agreement that crystallinity slightly increased with aging due to retrogradation. For TPS/TiO_2 composites the situation was different: ATR FTIR results indicated a slight increase in the crystallinity and ordering with time, while WAXS results proved a measurable decrease in the TiO_2-induced crystallinity

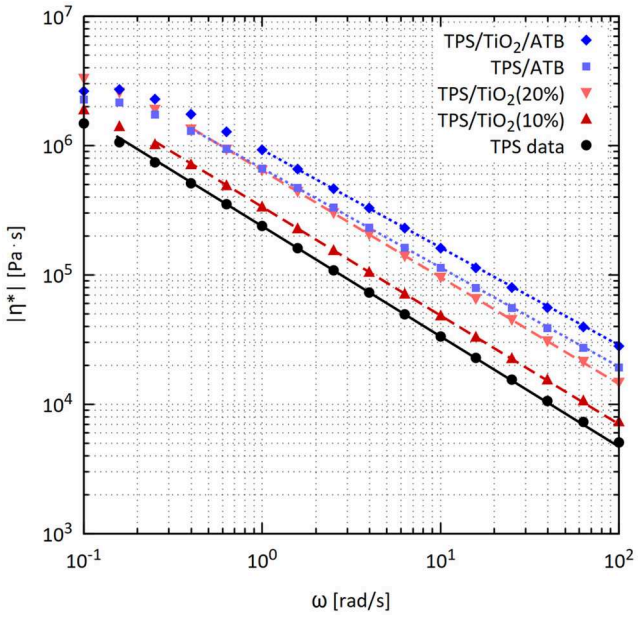

FIGURE 5 | Frequency sweep from oscillatory shear rheometry: absolute values of complex viscosities of the TPS/TiO_2/ATB composites at 120°C and strain of 0.05%, including comparison of the experimental points and their fitting with a power-law model (description of model in Ostafinska et al., 2017).

with time. This could be explained by the core-shell structure of the prepared samples. ATR FTIR collects signal from the thin shell, i.e., from the very surface layer at the top of the sample, where the concentration of the plasticizers during aging decreases. Consequently, the above-proposed destruction of metastable crystalline structure due to plasticizers was limited and the dominating effect was a crystallinity increase due to retrogradation. WAXS collects signal from the bulk, because the X-rays penetrate inside the specimen, where concentration of the plasticizers is high. According our tentative explanation from the previous paragraph, the high concentration of plasticizers destroys the proposed metastable, TiO_2-induced TPS crystalline structures. Therefore, the dominating effect was the small crystallinity decrease. The formation of metastable crystalline structures due to high concentration of filler was rather surprising and not observed for lower concentration of fillers in previous studies, but we should note that TPS matrices with such high filler concentration have not been characterized by WAXS in the literature so far.

Rheological Properties

The rheological properties of TPS/TiO_2/ATB composites measured in the oscillatory shear at 120°C are shown in **Figures 5**, **6**. The logarithmic dependence of the TPS complex viscosity ($|\eta^*|$) on the angular frequency (ω) showed a linear decrease almost in the entire 0.1–100 rad/s range. A slight curvature down appeared only for the lowest frequencies. The storage modulus (G') was larger than the loss modulus (G'') in the entire range of ω. G' grew linearly with frequency for ω above 0.4 rad/s in the logarithmic plot and curved down faintly with decreasing frequency for ω below 0.4 rad/s. This behavior corresponded to the slightly crosslinked polymers, physical gels or uncrosslinked polymers with high molecular weights, for which the Newtonian plateau in the viscosity and the crossing point of G' and G'' are shifted to a low ω (Mezger, 2014).

The complex viscosity ($|\eta^*|$) values of TPS/TiO_2 composites were very high in the entire range of frequencies (**Figure 5**), in agreement with previous studies (Della Valle et al., 1998; Deme et al., 2014; Ostafinska et al., 2017). The complex viscosities of TPS/TiO_2 exceeded the complex viscosity value for the pure TPS matrix. The storage and loss moduli of TPS/TiO_2 were higher than those of neat TPS in the entire frequency range. The enhancement of the rheological properties of TPS/TiO_2 with respect to neat TPS increased with the amount of TiO_2 in the composite. The shapes of the dependences of $|\eta^*|$, G' *and* G'' on ω for TPS/TiO_2 were essentially the same as those for neat TPS. There was no indication that TiO_2 formed a continuous physical network in TPS.

The previously studied composites with TiO_2 concentrations of up to 3% (Ostafinska et al., 2017) had the values of storage, loss, and complex modulus slightly lower than the corresponding values for pure TPS, which was attributed to the chain scissions of the TPS molecules at elevated temperatures. In this work, the moduli of the TPS/TiO_2 (10%) composites were already higher than those for TPS. This indicated that for a higher filler content, the reinforcing properties of the filler were already more dominant than the chain scissions of the TPS molecules at elevated temperature, resulting in the significantly higher moduli of the TPS/TiO_2 composites in comparison with the pure TPS matrix (**Figures 6A,B**).

The effect of the ATB addition on the rheological properties of TPS was more complex. Higher values of $|\eta^*|$, G' and G'' were found at ω above 1 rad/s for TPS/ATB (90/10) in comparison with TPS/TiO_2 (90/10); the same trend applied to TPS/TiO_2/ATB (80/10/10) in comparison with TPS/TiO_2 (80/20). In contrast to the TPS/TiO_2 composites, the shapes of the logarithmic plots of the rheological properties vs. ω for composites containing ATB differed remarkably from those for neat TPS. The decrease of $|\eta^*|$ with ω in the linear region of the logarithmic plot (above ω = 1 rad/s) was slower and the related increase in G' was steeper for the composites containing ATB than for neat TPS or for the TPS/TiO_2 composites. A decrease in the values of $|\eta^*|$ and G' for low frequencies with respect to the related values obtained by extrapolation from the linear regions of the logarithmic plots started at higher ω and was substantially higher for the composites with ATB than for neat TPS and TPS/TiO_2. This indicated that ATB enhanced the contribution of the elements with short relaxation times and suppressed the contribution of the elements with long relaxation times to the viscosity and elasticity of the composites. This was apparently a consequence of the complex, hydrogen-bond based interactions among starch, glycerol, and ATB.

Mechanical Properties

The dynamic moduli of TPS/TiO_2/ATB composites at room temperature (ω = 1.33 rad/s, deformation = 0.1%) are

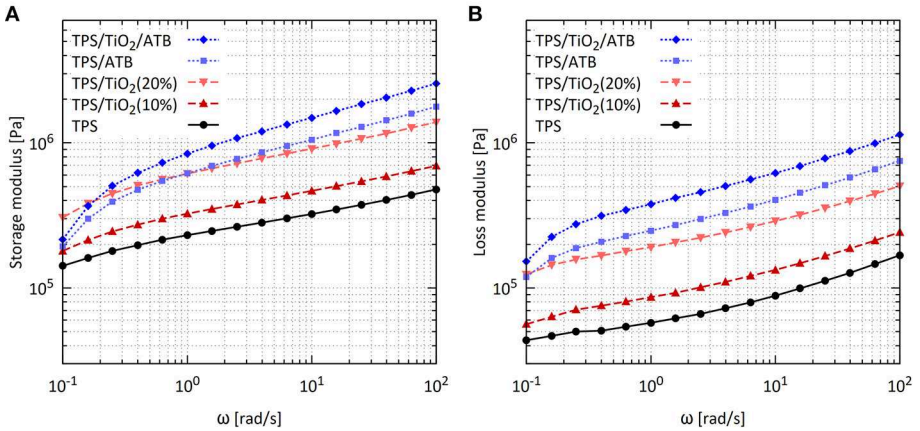

FIGURE 6 | Frequency sweeps from oscillatory shear rheometry: **(A)** Storage modulus G′ and **(B)** loss modulus G″ **(B)** of the TPS/TiO_2/ATB composites at 120°C and strain of 0.05%.

summarized in **Figure 7**. The storage moduli (G') and complex moduli ($|G^*|$) of all composites were higher than the corresponding moduli of the pure TPS matrix. With the addition of TiO_2 the storage moduli increased by 1.3 and 3 times for 10 and 20% of the filler, respectively. The modulus of the TPS/ATB samples was 20 times higher than that of TPS, confirming the strong interaction between ATB and TPS matrix. A further increase in the modulus of 1.4 times with respect to TPS/ATB (90/10) was obtained for the TPS/TiO_2/ATB (80/10/10) samples. This suggested that the influence of the filler content on the elastic modulus was approximately the same for both TPS (1.3× increase) and TPS/ATB (1.4× increase). Somewhat higher estimated standard deviations for the TPS/TiO_2 composites in comparison with the pure (and homogenous) matrix can be attributed to the fact that the mechanical properties are very sensitive to the homogeneity of material and also to the fact that TPS materials are sensitive to moisture content and aging (Della Valle et al., 1998).

Dynamic mechanical thermal analysis (DMTA) of the TPS/TiO_2/ATB composites was carried out in order to supplement room temperature measurements and to characterize the influence of TiO_2 and ATB on the phase changes in the TPS systems (**Figure 8**). Neat TPS systems after two-step preparation by SC + MM contained 30% of glycerol and 5% of residual water as evidenced by TGA (**Figure S6**). Their G'-curves (**Figure 8A**) showed behavior typical of gels with a low degree of crosslinking: above T_g, the elastic modulus curve clearly goes down, and G' is higher than G'' in the entire temperature range (**Figures 8A,B**) (Mezger, 2014, p. 195). These gel-like DMTA results can be attributed to the high-molecular weight branched amylopectin molecules. The loss modulus (G'') and the damping factor (tan(δ)) curves (**Figures 8B,C**) showed two local maxima corresponding to the two glass transition temperatures (T_g) typical of TPS with higher concentration of plasticizers (Mezger, 2014, p. 192). Generally, the addition of plasticizers to a polymer system decreases the T_g. A higher content of plasticizers may result in two glass transitions, indicating the presence of two separate phases with different plasticizer concentrations (Mezger, 2014, p. 196). In the specific case of TPS plasticized

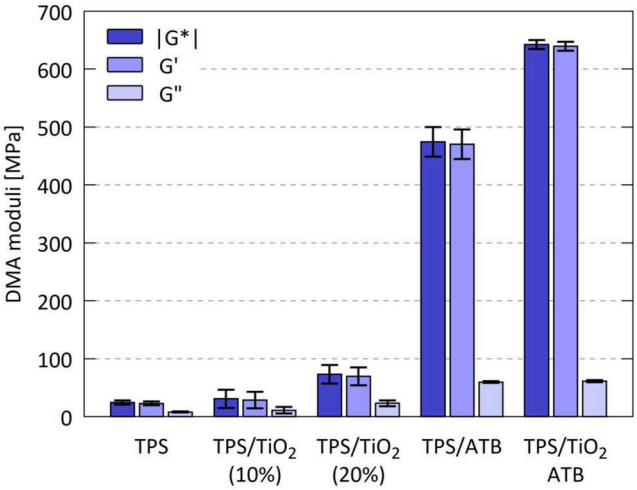

FIGURE 7 | Shear moduli (storage modulus G′, loss modulus G″, and complex modulus |G*|) from DMTA analysis of the TPS/TiO_2/ATB composites, determined at room temperature, angular frequency 1.33 rad/s and strain of 0.1%; error bars represent standard deviations.

with glycerol in combination with water, the two observed maxima were assigned to the "glycerol-rich phase" (below 0°C) and the "starch-rich phase" (also "amylopectin-rich phase" or "glycerol-poor phase"; above 0°C); their exact location and intensity depends on the preparation protocol (Viguie et al., 2007; Bertolini, 2010; Saiah et al., 2012; Balakrishnan et al., 2017; Sessini et al., 2018). It is worth noting that DMTA analysis turned out to be a more sensitive tool for T_g detection than the DSC method, which was used in our previous work (Ostafinska et al., 2017) on analogous systems, where DSC was able to detect the "glycerol-rich phase" glass transition but not the "starch-rich phase" glass transition.

The influence of the additives on the DMTA properties of the TPS/TiO_2/ATB systems illustrated in **Figure 8** corresponded quite well to the expected trends. The addition of the filler

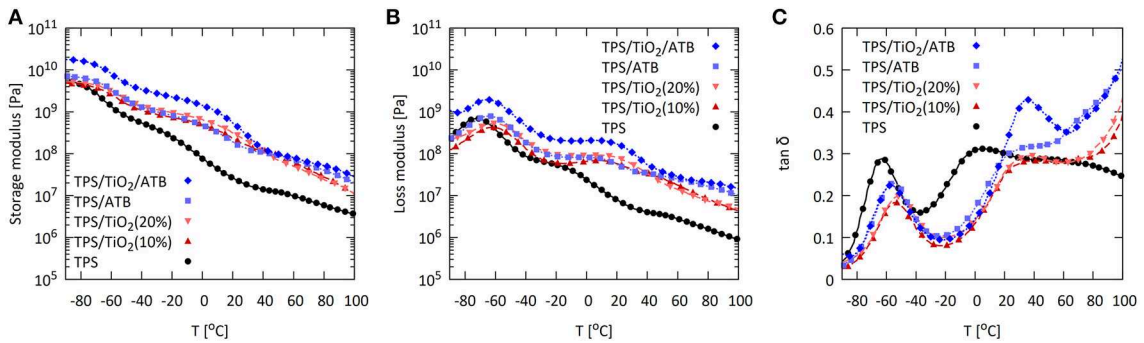

FIGURE 8 | Dynamic mechanical thermal analysis of the TPS/TiO_2/ATB composites at the angular frequency of 6.28 rad/s and strain of 0.05%: **(A)** Storage modulus G′, **(B)** loss modulus G″, and **(C)** damping factor tan(δ).

can strongly influence the overall stiffness of the composite (related to G') and the glass transition temperature of the matrix [related to the peaks of G'' and tan(δ)]. Typically, increasing filler concentration results in the shift of the G'-curve to higher values that is accompanied by the decreasing intensity and broadening of the G'' and tan(δ) peaks.

The stiffness of TPS (represented by absolute values of G' in the entire temperature range) increased both after the addition of the TiO_2 particles and ATB (**Figure 8A**). The only small exception were the lowest temperatures (at approximately −90°C), where the storage moduli of TPS and TPS/TiO_2 composites were approximately the same, while the ATB-containing systems exhibited higher G' at all temperatures. The increase in G' due to high-modulus inorganic TiO_2 particles was logical while the further G' increase after addition of organic ATB molecules appeared to arise from complex, and not-entirely understood interactions among the matrix, the TiO_2 particles and ATB, as discussed in the previous section dealing with rheology. Both the neat TPS matrix and all of the composites had storage moduli values higher than those of the loss moduli ($G' > G''$) in the entire temperature range (cf. **Figures 8A,B**), confirming the gel-like structure and physical stability of all systems (Ross-Murphy, 1995).

The two glass transition temperatures of the TPS composites (related to the G'' and tan(δ)curve peaks) showed similar changes (**Figures 8B,C**). The peaks corresponding to T_g of the "glycerol-rich phase" of all composites were slightly shifted toward higher temperatures (from −63°C for TPS to −55°C for the ATB composites and to −52°C for the TiO_2 composites; **Figure 8C**). Additionally, the peaks corresponding to the T_g values of the "starch-rich phase" were shifted toward higher temperatures for all of the composites (from 5°C for TPS to 35°C for the ATB composites and to 39°C for the TiO_2 composites) and the filler effect was even stronger. Therefore, the addition of both TiO_2 and ATB slightly hindered the mobility of the glycerol-rich phase (TiO_2 more than ATB) and strongly decreased the mobility of the "starch-rich phase" (both additives showed approximately the same effect). This effect was described in similar systems (Viguie et al., 2007; Sessini et al., 2018) and it was attributed to attractive interactions, such as hydrogen bonding between the additives and the TPS matrix, in the cases where all of the components (in our case: starch, glycerol, ATB vancomycin, and surfaces of the TiO_2 particles) contain –OH groups. Moreover, it was suggested that the T_g shift of the "starch-rich phase" was due to the lower molecular mobility of amylopectin chains in TPS (Viguie et al., 2007; Sessini et al., 2018).

Antibacterial Activity

TPS composites, such as TPS/ATB and TPS/TiO_2/ATB represent promising materials for the treatment of strong local infections. TPS is fully biocompatible and biodegradable and can be blended with other suitable biodegradable polymers (typically PCL) in order to adjust biodegradability rate and/or ATB release rate for given application. Inorganic particles, such as TiO_2 can be used to fine-tune the thermo-mechanical performance, as demonstrated in the previous sections above. However, it still must be determined whether the selected ATB (in our case: vancomycin) can survive the two-step sample preparation and retain its role as the active antimicrobial agent. In order to answer this question, two standard and well-established antimicrobial susceptibility tests were performed: tube dilution test and disk diffusion test (Jorgensen and Ferraro, 2009).

The tube test results are shown in **Figures 9A,B**. The test tubes were filled with water and loaded with a small piece of the TPS/ATB and TPS/TiO_2/ATB samples from which 32 mg/L of ATB was expected to be released within 24 h (Slouf et al., 2017). The concentration of 32 mg/L was selected as the maximal acceptable limit for most biomedical applications. The ATB-containing tubes were inoculated with a standardized bacterial suspension of *Staphylococcus aureus*. Following overnight incubation (ca. 18 h), the tubes were examined for visible bacterial growth as evidenced by turbidity. The bacterial broth culture remained clear in both tubes containing the systems with antibiotics (TPS/ATB and TPS/TiO_2/ATB; **Figure 9A**), proving that the released ATB could inhibit the bacterial growth. The control sample (pure TPS; **Figure 9B**) exhibited turbidity, evidencing the microbial growth.

The modified disk diffusion test (**Figures 9C–E**) confirmed the results obtained in the tube dilution test. The same fresh samples (similar to those used in the tube dilution tests)

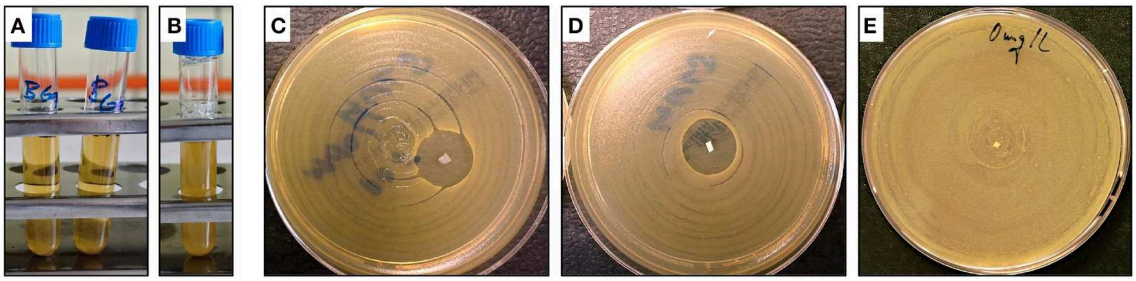

FIGURE 9 | Photographs showing the main results of antibacterial activity tests: **(A,B)** tube tests and **(C–E)** disk diffusion tests. Pictures of tubes **(A,B)** were made after 18 h of incubation: **(A)** shows translucent solutions of TPS/ATB (right) and TPS/TiO_2/ATB (left), while **(B)** shows turbid solution of control neat TPS sample. Pictures of disks **(C–E)** display clear inhibitory zones around small white rectangular samples of TPS/ATB **(C)** and TPS/ATB/TiO_2 **(D)**, while the control neat TPS sample exhibits no inhibitory zone **(E)**.

were pushed slightly into the agar plates inoculated with the *Staphylococcus aureus* reference strain (0.5 McFarland in saline). The plates were incubated for 18 h prior to the evaluation of the results. For TPS/ATB and TPS/TiO_2/ATB, typical inhibitory zones formed in the vicinity of the carrier indicated the release of the active ATB onto the agar medium (**Figures 9C,D**). This means that the antibiotics must have survived our SC + MM sample preparation and kept is antibacterial activity. Both inhibitory zones were similar, indicating that TiO_2 particles did not influence the ATB release. The control sample (pure TPS, **Figure 9E**) showed no inhibitory zone.

Both the tube test and the disk diffusion test demonstrated that a suitable ATB (such as vancomycin) that is resistant to elevated temperatures during solution casting (up to ca +80°C) and melt mixing (up to ca +120°C) can survive in the TPS in its active form. Moreover, the tests provided additional information regarding the different release rates of the TiO_2 particles and ATB molecules from TPS. The TiO_2 particles were not released from TPS to the solution and/or agar, as can be deduced from the fact that both solutions did not show visible white turbidity (**Figures 9A,B**). The particles must have been bonded well to the starch molecules by hydrogen bonds, because both components have an abundance of –OH groups. On the other hand, the ATB molecules can be released from the TPS structure even though ATB also contains –OH groups and interacts with TPS, as clearly evidenced by the rheological and thermomechanical measurements (**Figures 5–8**). However, for ATB, the osmotic pressure was evidently stronger than the effect of the hydrogen bonds that keep the ATB inside the thermoplastic starch.

Limitations of Current Study

TPS composites prepared in this work were characterized thoroughly regarding their morphology, rheology, and thermomechanical properties. The reproducibility of the preparation, the ideal homogeneity, and the full biodegradability make the prepared TPS composites suitable for biomedical applications for fast release of antibiotics during strong local infections. In potential applications, a temporary biodegradable TPS implant would release the ATB and then it would be safely degraded. However, the present work was focused on material characterization, whereas the antimicrobial susceptibility testing was somewhat simplified. In future work, two issues should be taken into consideration: the real biocompatibility of TiO_2 particles and the *bactericidal effect* of ATB (not only the *bacteriostatic effect* like in this work).

For the biocompatibility of the TiO_2 particles, the situation is not entirely clear. Numerous authors have reported that TiO_2 micro- and/or nanoparticles are a fully biocompatible material (Webster et al., 1999, 2000; Sengottuvelan et al., 2017), which is also broadly used as a food additive (Dudefoi et al., 2017). However, quite recently other researchers started to raise concerns about the potential toxicity of TiO_2 micro- and/or nanoparticles, particularly at the higher particle concentrations. On the one hand, Dudefoi et al. concluded that food grade TiO_2 particles did not significantly alter the human gut microbiota (Dudefoi et al., 2017) and Cervantes et al. found that TiO_2 thin films did not affect the mitochondrial function and proliferation of CHO-K1 cells (Cervantes et al., 2016). On the other hand, Fu et al. (2014) studied the generation of the reactive oxygen species (ROS) by various nanomaterials, which is an important nanotoxicity mechanism. They pointed out that the toxicity of the nanomaterials (related to generation of ROS) depends on many factors, such as the size, shape, particle surface, surface positive charges, surface-containing groups, particle dissolution, metal ion release from nanometals and nanometal oxides, UV light activation, aggregation, mode of interaction with the cells, inflammation, and the pH of the medium (Fu et al., 2014). Furthermore, Yu et al. (2017) studied the toxicity of nano-TiO_2 (both anatase and rutile with similar particle sizes) for mammalian cells. They found that the anatase nano-TiO_2 had a high affinity to proteins, whereas the rutile nano-TiO_2 had a high affinity to phospholipids. They proved that crystal phase-related surface affinity plays an important role for the nanotoxicity of different biomolecules (Yu et al., 2017). Therefore, the TPS/ATB composites are expected to be fully biocompatible, while the TPS/TiO_2/ATB composites should be further tested for the potential toxicity of the contained particles that would be released into the organism during the biodegradation.

For the antimicrobial activity, the current study unambiguously proved the *bacteriostatic effect* of the TPS/ATB

and TPS/TiO_2/ATB composites, but we did not attempt to determine the *minimal inhibitory concentration* (MIC) and the final *bactericidal effect* of the released ATB. More detailed tests, such as those described elsewhere (Schwalbe et al., 2007; Sedlarik, 2013), were beyond the scope of the present work. These tests will be carried out in our future study, in which we will employ the experience from this contribution and prepare TPS samples with various ATB concentrations.

CONCLUSIONS

In this work, we have demonstrated that our two-step preparation of thermoplastic starch (TPS; Ostafinska et al., 2017), which consists of solution casting followed by melt mixing, is suitable for reproducible preparation of TPS/TiO_2 composites with homogeneous dispersion of the filler, even at high filler concentrations (up to 20 wt.%). Moreover, the preparation procedure is suitable also for the preparation of TPS systems containing homogeneously dispersed antibiotics (ATB; here: vancomycin at 10 wt.%). The addition of both TiO_2 and ATB increased the viscosity of the TPS matrix ∼5×, as evidenced by rheological measurements. The interactions among TPS, TiO_2 particles, and ATB molecules resulted in the shifts of the glass transition temperatures to higher values and in the overall stiffening of the material (ca 25× increase in storage modulus of TPS/TiO_2/ATB with respect to neat TPS). Finally, standard antimicrobial susceptibility tests proved that neither thermal processing nor addition of TiO_2 influence the ATB, which remains active in both TPS/ATB and TPS/TiO_2/ATB composites. Therefore, we conclude that the prepared fully biodegradable TPS composites are a very promising material for biomedical applications involving local release of antibiotics.

DATA AVAILABILITY STATEMENT

The datasets generated for this study are available on request to the corresponding author.

AUTHOR CONTRIBUTIONS

MS designed the study, which was performed by AU (the sample preparation and characterization by light microscopy, important contribution to interpretation of rheological data), SK (electron microscopy), MN (rheometry and dynamical mechanical analysis), AZ (wide-angle X-ray scattering), JD (infrared microscopy), PF and ON (antimicrobial susceptibility testing). ZK contributed to the sample preparation and data interpretation. AU with the help of MS interpreted the results prepared a draft of the manuscript. MS finalized and submitted the manuscript.

FUNDING

Financial support through grants NV15-31269A (MZ CR), TE01020118 (TA CR), TN01000008 (TA CR), and POLYMAT LO1507 (MSMT, NPU I) is gratefully acknowledged.

ACKNOWLEDGMENTS

The authors would like to thank to Jirina Hromadkova for her technical assistance during SEM measurements.

SUPPLEMENTARY MATERIAL

The Supplementary Material for this article can be found online at: https://www.frontiersin.org/articles/10.3389/fmats.2020.00009/full#supplementary-material

REFERENCES

Abral, H., Basri, A., Muhammad, F., Fernando, Y., Hafizulhaq, F., Mahardika, M., et al. (2019). A simple method for improving the properties of the sago starch films prepared by using ultrasonication treatment. *Food Hydrocolloid.* 93 276–283. doi: 10.1016/j.foodhyd.2019.02.012

Aichholzer, W., and Fritz, H.-G. (1998). Rheological characterization of thermoplastic starch materials. *Starch* 50, 77–83. doi: 10.1002/(SICI)1521-379X(199803)50:2/3<77::AID-STAR77>3.0.CO;2-P

Ali, A., Xie, F., Liu, H., Meng, L., Khalid, S., and Chen, L. (2018). Preparation and characterization of starch-based composite films reinforced by polysaccharide-based crystals. *Compos. Part B* 133, 122–128. doi: 10.1016/j.compositesb.2017.09.017

Altskar, A., Andersson, R., Boldizar, A., Koch, K., Stading, M., Rigdahl, M., et al. (2008). Some effects of processing on the molecular structure and morphology of thermoplastic starch. *Carbohydr. Polym.* 71, 591–597. doi: 10.1016/j.carbpol.2007.07.003

Ao, Z., and Jane, J. (2007). Characterization and modeling of the A- and B-granule starches of wheat, triticale, and barley. *Carbohydr. Polym.* 67, 46–55. doi: 10.1016/j.carbpol.2006.04.013

Balakrishnan, P., Sreekala, M. S., Kunaver, M., Huskic, M., and Thomas, S. (2017). Morphology, transport characteristics and viscoelastic polymer chain confinement in nanocomposites based on thermoplastic potato starch and cellulose nanofibers from pineapple leaf. *Carbohydr. Polym.* 169, 176–188. doi: 10.1016/j.carbpol.2017.04.017

Bertolini, A. (2010). *Starches: Characterization, Properties, and Applications*. Boca Raton, FL: Taylor & Francis Group, LLC.

Biliaderis, C. G. (2009). "Structural transitions and related physical properties of starch," in *Starch. Chemistry and Technology, A Volume in Food Science and Technology, 3rd Edn.*, eds J. BeMiller and R. Whistler (Cambridge, MA: Academic press), 293–372. doi: 10.1016/B978-0-12-746275-2.00008-2

Boccaccini, A. R., and Blaker, J. J. (2006). Poly(D,L-lactide) (PDLLA) foams with TiO_2 nanoparticles and PDLLA/TiO_2-Bioglass foam composites for tissue engineering scaffolds. *J. Mater. Sci.* 41, 3999–4008. doi: 10.1007/s10853-006-7575-7

Boccaccini, A. R., Gerhardt, L.-C., Rebeling, S., and Blaker, J. J. (2005). Fabrication, characterisation and assessment of bioactivity of poly(D,L lactid acid) (PDLLA)/TiO_2 nanocomposite films. *Compos. Part A* 36, 721–727. doi: 10.1016/j.compositesa.2004.11.002

Campos, A., Senta Neto, A. R., Rodrigues, V. B., Luchesi, B. R, Moreira, F. K. V., Correa, A. C., et al. (2017). Bionanocomposites produced from cassava starch and oil palm mesocarp cellulose nanowhiskers. *Carbohydr. Polym.* 175, 330–336. doi: 10.1016/j.carbpol.2017.07.080

Campos-Requena, V. H., Rivas, B. L., Perez, M. A, Figueroa, C. R., Figueroa, N. E., and Sanfuentes, E. A. (2017). Thermoplastic starch/clay nanocomposites loaded with essential oil consituents as packaging

for strawberries–*in vivo* entimicrobial synergy over *Botrytis cinerea*. *Postharvest Biol. Technol.* 129, 29–36. doi: 10.1016/j.postharvbio.2017.03.005

Capron, I., Robert, P., Colonna, P., Brogly, M., and Planchot, V. (2007). Starch in rubbery and glassy states by FTIR spectroscopy. *Carbohydr. Polym.* 68, 249–259. doi: 10.1016/j.carbpol.2006.12.015

Carvahlo, A. J. F., Curvelo, A. A. S., and Agnelli, J. A. M. (2001). A first insight of thermoplastic starch and kaolin. *Carbohydr. Polym.* 45, 189–194. doi: 10.1016/S0144-8617(00)00315-5

Cervantes, B., Lopez-Huerta, F., Vega, R., Hernandez-Torres, J., Garcia-Gonzalez, L., Salceda, E., et al. (2016). Cytotoxicity evaluation of anatase and rutile TiO_2 thin films on CHO-K1 cells *in vitro*. *Materials* 9:619. doi: 10.3390/ma9080619

Dai, H., Chang, P., Yu, J., and Ma, X. (2008). N,N-Bis(2-hydroxyethyl)formamide as a new plasticizer for thermoplastic starch. *Starch* 60, 676–684. doi: 10.1002/star.200800017

Dai, H., Sheng, X., An, L., Liu, N., Yu, J., and Ma, X. (2012). Preparation and properties of thermoplastic starch/montmorillonite nanocomposites using N,N-bis(2-hydroxyethyl)formamide as a new additive. *Polym. Compos.* 33, 225–231. doi: 10.1002/pc.22142

Della Valle, G., Buleon, A., Carreau, P. J., Lavoie, P. A., and Vergnes, B. (1998). Relationship between structure and viscoelastic behavior of plasticized starch. *J. Rheol.* 42, 507–525. doi: 10.1122/1.550900

Deme, F., Peuvrel-Disdier, E., and Vergnes, B. (2014). Rheology and morphology of polyester/thermoplastic flour blends. *J. Appl. Polym. Sci.* 131:40222. doi: 10.1002/app.40222

Dudefoi, W., Moniz, K., Allen-Vercoe, E., Ropers, M.-H., and Walker, V.K. (2017). Impact of food grade and nano-TiO_2 particles on a human intestinal community. *Food Chem. Toxicol.* 16, 242–249. doi: 10.1016/j.fct.2017.05.050

Dufresne, A., and Castano, J. (2017). Polysaccharide nanomaterial reinforced starch nanocomposites: a review. *Starch* 69:1500307. doi: 10.1002/star.201500307

Fei, P., Shi, Y., Zhou, M., Cai, J., Tang, S., and Xiong, H. (2013). Effects of nano-TiO_2 on the properties and stuctures of starch/poly(ε-caprolactone) composites. *J. Appl. Polym. Sci.*130, 4129–4136. doi: 10.1002/app.39695

Fu, P. P, Xia, Q., Hwang, H.-M., Ray, P. C., and Yu, H. (2014). Mechanisms of nanotoxicity: generation of reactive oxygen species. *J. Food Drug Anal.* 22, 64–75. doi: 10.1016/j.jfda.2014.01.005

Ghavimi, S. A. A., Ebrahimzadeh, M. H., Shokrgozar, M. A., Solati-Hashjin, M., and Osman, N. A. A. (2015). Effect of starch content on the biodegradation of polycaprolactone/starch composite for fabricating *in situ* pore-forming scaffolds. *Polym. Test.* 43, 94–102. doi: 10.1016/j.polymertesting.2015.02.012

Gupta, K. K., Kundan, A., Mishra, P. K., Srivastava, P., Mohanty, S., Singh, N. K., et al. (2012). Polycaprolactone composites with TiO_2 for potential nanobiomaterials: tunable properties using different phases. *Phys. Chem. Chem. Phys.* 14, 12844–12853. doi: 10.1039/c2cp41789h

Guz, L., Candal, R., and Goyanes, S. (2017). Size effect of ZnO nanorods on physicochemical properties ofplasticized starch composites. *Carbohydr. Polym.* 157, 1611–1619. doi: 10.1016/j.carbpol.2016.11.041

Huang, M., Yu, J., and Ma, X. (2005). Ethanolamine as a novel plasticizer for thermoplastic starch. *Polym. Degrad. Stab.* 90, 501–507. doi: 10.1016/j.polymdegradstab.2005.04.005

Ilyas, R. A., Sapuan, S. M., Atiqah, A., Ibrahim, R., Abral, H., Ishak, M. R., et al. (2019). Sugar palm (*Arenga pinnata* [Wurmb.] Merr) starch films containing sugar palm nanofibrillated cellulose as reinforcement: water barrier properties. *Polym. Compos.* doi: 10.1002/pc.25379. [Epub ahead of print].

Ilyas, R. A., Sapuan, S. M., Ishak, M. R., and Zainudin, E. S. (2018). Development and characterization of sugar palm nanocrystalline cellulose reinforced sugar palm starch bionanocomposites. *Carbohydr. Polym.* 202, 186–202. doi: 10.1016/j.carbpol.2018.09.002

Javanbakht, S., and Namazi, H. (2017). Solid state photoluminescence thermoplastic starch film containing graphene quantum dots. *Carbohydr. Polym.* 176, 220–226. doi: 10.1016/j.carbpol.2017.08.080

Jorgensen, J. H., and Ferraro, M. J. (2009). Antimicrobial susceptibility testing: a review of general principles and contemporary practices. *Clin. Infect. Dis.* 49, 1749–1755. doi: 10.1086/647952

Kargarzadeh, H., Johar, N., and Ahmad, I. (2017). Starch biocomposite film reinforced by multiscale rice husk fiber. *Compos. Sci. Technol.* 151, 147–155. doi: 10.1016/j.compscitech.2017.08.018

Kelnar, I., Kapralkova, L., Brozova, L., Hromadkova, J., and Kotek, J. (2013). Effect of chitosan on the behaviour of the wheat B-starch nanocomposite. *Ind. Crops Prod.* 46, 186–190. doi: 10.1016/j.indcrop.2013.01.030

Kuswandi, B. (2017). Environmental friendly food nano-packaging. *Environ. Chem. Lett.* 15, 205–221. doi: 10.1007/s10311-017-0613-7

Li, G., Sarazin, P., and Favis, B. D. (2008). The relationship between starch gelatization and morphology control in melt-processed polymer blends with thermoplastic starch. *Macromol. Chem. Phys.* 209, 991–1002. doi: 10.1002/macp.200700637

Liu, G., Gu, Z., Hong, Y., Cheng, L., and Li, C. (2017). Electrospun starch nanofibres: recent advances, challenges, and strategies for potential pharmaceutical applications. *J. Controlled Release* 252, 95–107. doi: 10.1016/j.jconrel.2017.03.016

Liu, S., Li, X., Chen, L., Li, L., Li, B., and Zhu, J. (2017). Understanding physicochemical properties changes from multi-scale structures of starch/CNT nanocomposite films, *Int. J. Biol. Macromol.* 104, 1330–1337. doi: 10.1016/j.ijbiomac.2017.05.174

Liu, Y. X., Fan, L. L., Mo, X. Z., Yang, F., and Pang, J. Y. (2018). Effects of nanosilica on retrogradation properties and structures of thermoplastic cassava starch. *J. Appl. Polym. Sci.* 135:45687. doi: 10.1002/app.45687

Mezger, T. G. (2014). *The Rheology Handbook, 4th Edn.* Hannover: Vincentz Network GmbH.

Mina, J. H., Valadez, A., Herrera-Franco, P. J., and Toledano, T. (2012). Infuence of aging timeon the structural changes of cassava thermoplastic starch. *Mater. Res. Soc. Symp. Proc.* 1372, 21–27. doi: 10.1557/opl.2012.129

Mofokeng, J. P., and Luyt, A. S. (2015a). Morphology and thermal degradation studies of melt-mixed poly(lactic acid) (PLA)/poly(ε-caprolactone) (PCL) biodegradable polymer blend nanocomposites with TiO_2 as filler. *Polym. Test.* 45, 93–100. doi: 10.1016/j.polymertesting.2015.05.007

Mofokeng, J. P., and Luyt, A. S. (2015b). Dynamic mechanical properties of PLA/PHBV, PLA/PCL, PHBV/PCL blends and their nanocomposites with TiO_2 as nanofiller. *Thermochim. Acta* 613, 41–53. doi: 10.1016/j.tca.2015.05.019

Oleyaei, S. A., Almasi, H., Ghanbarzadeh, B., and Moayedi, A. A. (2016a). Synergistic reinforcing effect of TiO_2 and montmorillonite on potato starch nanocomposite films: thermal, mechanical and barrier properties. *Carbohydr. Polym.* 152, 253–262. doi: 10.1016/j.carbpol.2016.07.040

Oleyaei, S. A., Zahedi, Y., Ghanbarzadeh, B., and Moayedi, A. A. (2016b). Modification of physicochemical and thermal properties of starch films by incorporation of TiO_2 nanoparticles. *Int. J. Biol. Macromol.* 89, 256–264. doi: 10.1016/j.ijbiomac.2016.04.078

Olivato, J. B., Marini, J., Yamashita, F., Pollet, E., Grossmann, M. V. E., and Averous, L. (2017). sepiolite as a promising nanoclay for nano-biocomposites based on starch and biodegradable polyester. *Mater. Sci. Eng. C* 70:296302. doi: 10.1016/j.msec.2016.08.077

Ostafinska, A., Fortelny, I., Nevoralova, M., Hodan, J., Kredatusova, J., and Slouf, M. (2015). Synergistic effects in mechanical properties of PLA/PCL blends with optimized composition, processing, and morphology. *RSC Adv.* 5, 98971–98982. doi: 10.1039/C5RA21178F

Ostafinska, A., Mikesova, J., Krejcikova, S., Nevoralova, M., Sturcova, A., Zhigunov, A., et al. (2017). Thermoplastic starch composites with TiO_2 particles: preparation, morphology, rheology and mechanical properties. *Int. J. Biol. Macromol.* 101, 273–282. doi: 10.1016/j.ijbiomac.2017.03.104

Pelissari, F. M., Andrade-Mahecha, M. M., Amaral Sobral, P. J., and Menegalli, F. C. (2017). Nanocomposites based on banana starch reinforced with cellulose nanofibers isolated from banana peels. *J. Colloid Interface Sci.* 505, 154–167. doi: 10.1016/j.jcis.2017.05.106

Pushpadass, H., Marx, D. B., and Hanna, M. A. (2008). Effects of extrusion temperature and plasticizers on the physical and functional properties of starch films. *Starch* 60, 527–538. doi: 10.1002/star.200800713

Rappenecker, G., and Zugenmaier, P. (1981). Detailed refinement of the crystal structure of Vh-amylose. *Carbohydr. Res.* 89, 11–19. doi: 10.1016/S0008-6215(00)85225-8

Razali, S. M., Yusoff, M., Ramle, S. F. M., Bhat, I. U. H., Iman, A. H. M., and Razali, A. M. H. (2016). The potential of *Donax grandis* hypodermal fiber as a reinforcement in starch-based composite. *J. Polym. Mater.* 33, 677–684.

Ross-Murphy, S. B. (1995). Structure-property relationships in food biopolymer gels and solutions. *J. Rheol.* 39, 1451–1463. doi: 10.1122/1.550610

Saiah, R., Gatin, R., and Sreekumar, P. A. (2012). "Properties and biodegradation nature of thermoplastic starch," in *Thermoplastic Elastomers*, ed A. El-Sonbati (London: InTech), 57–78. doi: 10.5772/35348

Sarka, E., and Dvoracek, V. (2017). New processing and applications of waxy starch (a review). *J. Food Eng.* 206, 77–87. doi: 10.1016/j.jfoodeng.2017.03.006

Sarka, E., Krulis, Z., Kotek, J., Ruzek, K. A., Bubnik, Z., and Ruzkova, M. (2011). Application of wheat B-starch in biodegradable plastic materials. *Czech J. Food Sci.* 29, 232–242. doi: 10.17221/292/2010-CJFS

Sarka, E., Krulis, Z., Kotek, J., Ruzek, L., Vorisek, K., Kolacek, K., et al. (2012). Composites containing acetylated wheat B-starch for agriculture applications. *Plant Soil Environ.* 58, 354–359. doi: 10.17221/287/2012-PSE

Schwalbe, R., Steele-Moore, L., and Goodwin, A. C. (2007). *Antimicrobial Susceptibility Testing Protocols*. Boca Raton, FL: CRC Press, Taylor & Francis Group. doi: 10.1201/9781420014495

Sedlarik, V. (2013). *Antimicrobial Modifications of Polymers, Biodegradation*. Rolando Chamy and Francisca Rosenkranz, IntechOpen. Available online at: https://www.intechopen.com/books/biodegradation-life-of-science/antimicrobial-modifications-of-polymers

Sengottuvelan, A., Balasubramanian, P., Will, J., and Boccaccini, A. R. (2017). Bioactivation of titanium dioxide scaffolds by ALP-functionalization. *Bioact. Mater.* 2, 108–115. doi: 10.1016/j.bioactmat.2017.02.004

Sessini, V., Arriera, M. P., Fernandez-Torres, A., and Peponi, L. (2018). Humidity-activated shape memory effect on plasticized starch-based biomaterials. *Carbohydr. Polym.* 179, 93–99. doi: 10.1016/j.carbpol.2017.09.070

Slouf, M., Krulis, Z., Ostafinska, A., Nevoralova, M., Krejcikova, S., Horak, et al. (2017). *Polymerní Termoplastická Biodegradovatelná Kompozice pro Výrobu VložEk k Léčení a Prevenci Lokálních Infektu a Zpusob Její Prípravy*. Czech Patent CZ 307056. Prague: Czech Patent and Trademark Office.

Soest, J. J. G., Hulleman, S. H. D., de Wit, D., and Vliegenthart, J. (1996). Crystallinity in starchbioplastics. *Ind. Crops Prod.* 5, 11–22. doi: 10.1016/0926-6690(95)00048-8

Svagan, A. J., Hedenqvist, M. S., and Berglund, I. (2009). Reduced water vapour sorption in cellulose nanocomposites with starch matrix. *Compos. Sci. Technol.* 69, 500–506. doi: 10.1016/j.compscitech.2008.11.016

Tamjid, E., Bagheri, R., Vossoughi, M., and Simchi, A. (2011). Effect of TiO_2 morphology on *in vitro* bioactivity of polycaprolactone/TiO_2 nanocomposites. *Mater. Lett.* 65, 2530–2533. doi: 10.1016/j.matlet.2011.05.037

Vackova, T., Kratochvil, J., Ostafinska, A., Krejcikova, S., Nevoralova, M., and Slouf, M. (2017). Morphology, crystallization kinetics and rheology of PCL composites with TiO_2-based nanoparticles. *Polym. Bull.* 74, 445–464. doi: 10.1007/s00289-016-1723-2

Viguie, J., Molina-Boisseau, S., and Dufresne, A. (2007). Processing and characterization of waxy maize starch films plasticized by sorbitol and reinforced with starch nanocrystals. *Macromol. Biosci.* 7, 1206–1216. doi: 10.1002/mabi.200700136

Visakh, P. M., Mathew, P. A., Oksman, K., and Thomas, S. (2012). "Starch-basedbionanocomposites: processing and properties," in *Polysaccharide Building Blocks: A Sustainable Approach to the Developmentof Renowable Biomaterials*, eds Y. Habibi and L. A. Lucia (Hoboken, NJ: John Wiley & Sons, Inc.), 287–306. doi: 10.1002/9781118229484.ch11

Wang, S., Li, C., Copeland, L., Niu, Q., and Wang, S. (2015). Starch retrogradation: a comprehensive review. *Compr. Rev. Food. Sci. Food Saf.* 14, 568–585. doi: 10.1111/1541-4337.12143

Warren, F. J., Gidley, M. J., and Flanagan, B. M. (2016). Infrared spectroscopy as a tool to characterise starch ordered structure—a joint FTIR–ATR, NMR, XRD and DSC study. *Carbohydr. Polym.* 139, 35–42. doi: 10.1016/j.carbpol.2015.11.066

Webster, J., Ergun, C., Doremus, R. H., Siegel, R. W., and Bizios, R. (2000). Enhanced functions of osteoblasts on nanophase ceramics. *Biomaterials* 21, 1803–1810. doi: 10.1016/S0142-9612(00)00075-2

Webster, J., Siegel, W., and Bizios, R. (1999). Osteoblast adhesion on nanophase ceramics. *Biomaterials* 20, 1221–1227. doi: 10.1016/S0142-9612(99)00020-4

Wojdyr, M. (2010). Fityk: a general-purpose peak fitting program. *J. Appl. Cryst.* 43, 1126–1128. doi: 10.1107/S0021889810030499

Xie, F., Halley, P. J., and Averous, L. (2012). Rheology to understand and optimize processibility, structures and properties of starch polymeric materials. *Prog. Polym. Sci.* 37, 595–623. doi: 10.1016/j.progpolymsci.2011.07.002

Xie, F., Pollet, E., Halley, P. J., and Averous, L. (2013). Starch-based nano-biocomposites. *Prog. Polym. Sci.* 38, 1590–1628. doi: 10.1016/j.progpolymsci.2013.05.002

Yu, Q., Wang, H., Peng, Q., Li, Y., Liu, Z., and Li, M. (2017). Different toxicity of anatase and rutile TiO_2 nanoparticles on macrophages: Involvement of difference in affinity to proteins and phospholipids. *J. Hazard. Mater.* 335, 125–134. doi: 10.1016/j.jhazmat.2017.04.026

Yun, Y.-H., Youn, Y.-N., Yoon, S.-D., and Lee, J.-U. (2012). Preparation and physical properties of starch-based nanocomposite films with the addition of titanium oxide nanoparticles. *J. Ceram. Process. Res.* 13, 59–64.

Zobel, H. F., French, A. D., and Hinckle, M. E. (1967). X-Ray diffraction of oriented amylose fibers. II. Structure of V amylose. *Biopolymers* 5, 837–845. doi: 10.1002/bip.1967.360050906

Conflict of Interest: The authors declare that the research was conducted in the absence of any commercial or financial relationships that could be construed as a potential conflict of interest.